IEEE Access
Multidisciplinary | Rapid Review | Open Access Journal

Received 2 February 2024, accepted 17 February 2024, date of publication 20 February 2024, date of current version 4 March 2024.

Digital Object Identifier 10.1109/ACCESS.2024.3368144

RESEARCH ARTICLE

Magnetic Levitation Guiding System of a Ropeless Elevator for Semiconductor Wafer Vertical Transport: Experimental Evaluation

CHANG-WAN HA, (Member, IEEE), SUNGHO JUNG, (Member, IEEE), JINSEONG PARK, (Member, IEEE), AND JAEWON LIM, (Member, IEEE)
Department of AI Machinery, Korea Institute of Machinery and Materials (KIMM), Daejeon 34103, Republic of Korea

Corresponding author: Jaewon Lim (einses@kimm.re.kr)

This work was supported by the National Research Council of Science and Technology under Project "Development of Core Technologies for Robot General Task Artificial Intelligence (RoGeTA) Framework to Implement Various Daily Services" under Grant NK248G.

ABSTRACT A novel design of a magnetic levitation (maglev) ropeless elevator for semiconductor wafer vertical transport is newly presented. To satisfy high cleanliness during vertical transport of the wafer, linear motor lifting and maglev guiding are desirable instead of the conventional rope lifting and wheel-based guiding method. Owing to the physically noncontact maglev guiding, particle-free and high-speed operation can be achieved with remarkable ride quality. In this paper, practical challenges for wafer transport, such as the eccentricity of the mass center from the actuating axis, severe acceleration/deceleration conditions as well as periodic large disturbances from normal forces of the linear motor, resonance of the elevator, and manufacturing tolerance of the guide rail, are further considered to satisfy the ride performance in wafer transport by designing a robust feedback controller with a loop shaping technique. A full-scale maglev ropeless elevator was constructed to experimentally validate the effectiveness of the proposed method. The experimental results demonstrated excellent magnetic levitation guiding performance in 5 degrees of freedom, with a maximum airgap fluctuation of 227 μm under harsh lifting conditions ($V_{max} = 2600$ mm/s).

INDEX TERMS Magnetic levitation (maglev), guiding system, ropeless elevator, semiconductor, wafer vertical transport, motion control, robust control, loop-shaping, electromagnetic field analysis, vibration analysis.

I. INTRODUCTION

Ropeless elevators with a magnetic levitation (maglev) guiding system have been touted as a good solution for vertical transportation due to their better dynamic behavior and contactless operation. An elevator mainly consists of lifting and guiding systems. Conventional elevators use ropes to lift the elevator cabin in the vertical direction and use rollers to guide the cabin in the horizontal direction [1], [2]. Therefore, in conventional elevators, physical contact always occurs, so the ride quality is significantly deteriorated, especially in high-speed operation, and wear and dust are consistently generated.

Compared to the rope lifting method, linear motor lifting has excellent dynamic characteristics. Thus, it can operate rapidly, and it can control multiple elevators independently in a single guideway, which significantly improves the transport capacity. Compared to the wheel-based guiding method, physically noncontact maglev guiding does not generate wear or dust and does not require lubrication. Moreover, maglev guiding is advantageous for achieving a high level of ride quality through active feedback control even in the presence of unevenness of the guide rail and harsh driving conditions.

In previous studies on linear motor lifting instead of the conventional rope lifting method, various attempts have been made to independently control multiple elevators in a single guideway and realize a high level of dynamic characteristics. ThyssenKrupp Corp. utilized a linear synchronous motor for lifting a passenger elevator and newly presented a rotary

The associate editor coordinating the review of this manuscript and approving it for publication was Agustin Leobardo Herrera-May.

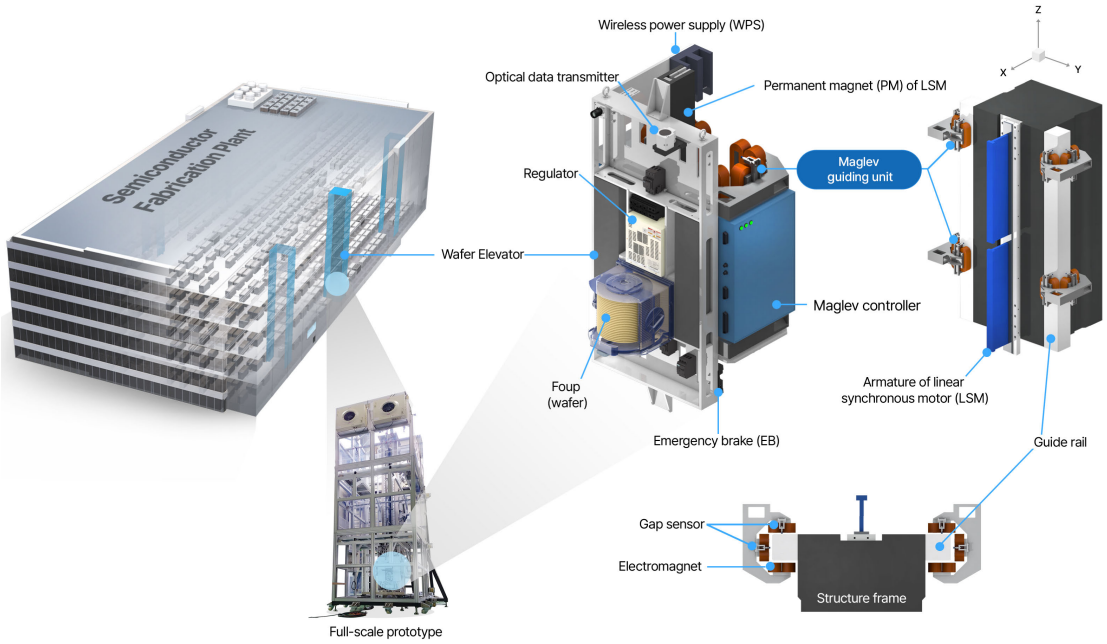

FIGURE 1. System configuration of the maglev ropeless elevator for wafer vertical transport.

branch system to enable horizontal operation such that the concept of transportation has been expanded, and recently, test operation was started in a full-scale test tower [3]. Onat et al. designed a new permanent magnet synchronous linear motor to enable both thrust and brake mechanisms by decoupling the magnetic field, forming a safety system integrated into the lifting system [4]. Okamoto and Takahashi presented topology optimization of the coreless-type linear synchronous motor to reduce the ripple of the lifting force through density and ON/OFF methods [5]. Zahid et al. designed a dual mover yokeless multitooth permanent magnet flux switching motor to achieve a high and cost-effective lifting force [6]. Lim and Krishnan [7] and Wang et al. [8] adopted a linear switched reluctance motor for a ropeless elevator and experimentally validated it with a prototype.

In previous studies on physically noncontact maglev guiding, various attempts have been made to realize a high level of ride quality that cannot be reached by conventional wheel-based guiding methods. Toshiba Corp. presented a maglev guiding system called MagSus (magnetic suspension) for rope-driven passenger elevators, which actively controls the horizontal behavior of the elevator to minimize the vibration caused by the unevenness of the guide rail during high-speed operation [9]. Alipour et al. improved the control robustness and driving performance by applying a proportional-integral-derivative (PID) sliding mode controller to the maglev guiding system and verified its effectiveness with a MATLAB simulation [10]. Schmülling et al. presented multidegree guide position control of an overdetermined system by employing the pole placement method [11]. The elevator posture control using the maglev guiding system was experimentally evaluated by realizing a test bench operated by ropes [12] or linear synchronous motors [13]. Appunn and Hameyer also presented a combined unit of a maglev guiding system and a contactless power supply with the introduction of soft magnetic composites [14].

In this paper, a ropeless elevator equipped with a maglev guiding system and a linear synchronous motor is designed for semiconductor manufacturing processes that require high cleanliness. Unlike passenger elevators, in the wafer transport elevator, for wafer handling operations, the major components of the elevator, including the linear motor and maglev guiding system, cannot be placed on the front, left, or right sides of the elevator. Therefore, the maglev guiding system must be placed on the backside of the elevator, and thus there is inevitably eccentricity of the mass center from the actuating axis of the maglev guiding system (see the backpack-topology in [13]). Moreover, the lifting conditions are harsh, involving extremely high accelerations to maximize manufacturing capabilities. The severe motion with eccentricity of the mass center generates a large amount of pitching motion of the elevator. Additionally, for practical applications, periodic large disturbances from normal forces of the linear motor, resonance of the elevator, and unevenness of the guide rail should be considered. Therefore, we designed robust feedback control based on the loop shaping technique. The performance of our control method was experimentally verified with a 6 m-long maglev ropeless elevator prototype.

This paper is the first attempt to experimentally demonstrate maglev guiding performance at the hundreds of micrometer level under harsh lifting conditions, involving abrupt acceleration, for the vertical transport of a semiconductor wafer in the presence of practical challenges.

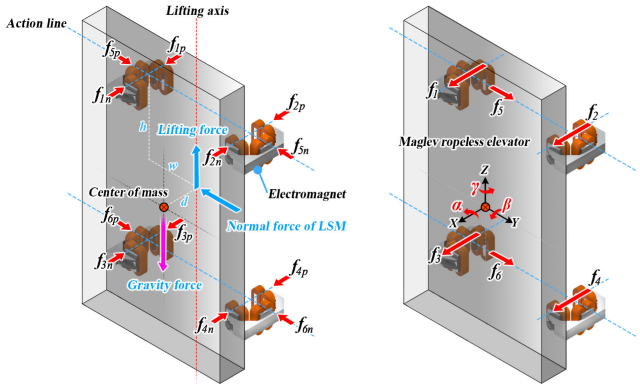

FIGURE 2. (Left) Individual forces and (Right) superposed forces of all maglev guiding units.

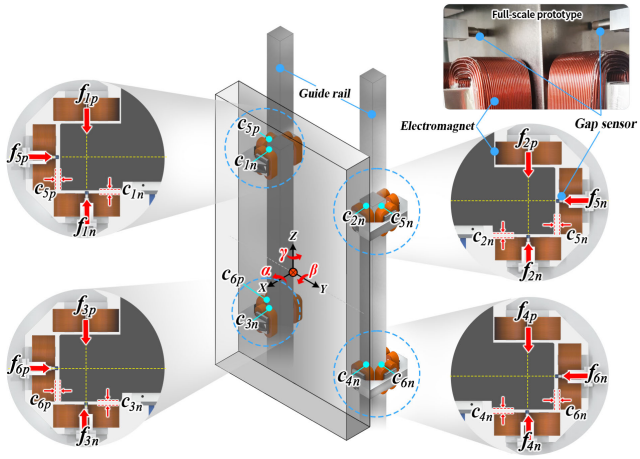

FIGURE 3. Airgaps measured by gap sensors.

The rest of this paper is organized as follows. In Section II, the configuration of the 6 m-long maglev ropeless elevator prototype is presented. The maglev guiding system and controller are designed in Section III. Experimental evaluation of our proposed control method is performed in Section IV, and concluding remarks are presented in Section V.

II. DEVELOPMENT OF A MAGLEV ROPELESS ELEVATOR

The maglev ropeless elevator consists of a maglev guiding system that controls the motion of the 5 degrees of freedom (DOFs) and a linear synchronous motor (LSM) that handles the lifting axis and compensates gravity force. A 6 m-long prototype equipped with the maglev guiding system, the linear motor, and a support frame is shown in Fig. 1, whose maximum moving stroke in the Z-direction is 4.2 m. A schematic diagram of the maglev ropeless elevator and its major components are shown in Fig. 1. The major components mounted on the elevator include maglev guiding units, maglev controllers, the permanent magnet of the LSM, a wireless power transmission system (WPS), power converters, an optical communication system, and emergency brakes.

To control the horizontal behavior of the elevator, the maglev guiding system consists of four maglev guiding

TABLE 1. Major design parameters of the maglev guiding units.

Parameter	Description	Value	
		X-axis	Y-axis
f_0	Nominal force	335 N	173 N
i_0	Nominal current	2 A	1 A
c_0	Nominal airgap	0.9 mm	0.7 mm
N_e	Number of windings	270 turns	
A	Pole area	1200 mm^2	

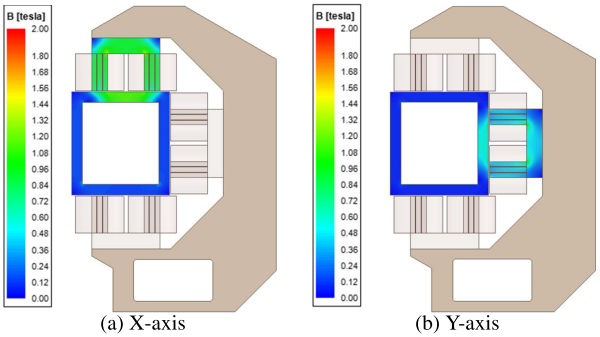

FIGURE 4. Electromagnetic field analysis of the maglev guiding unit.

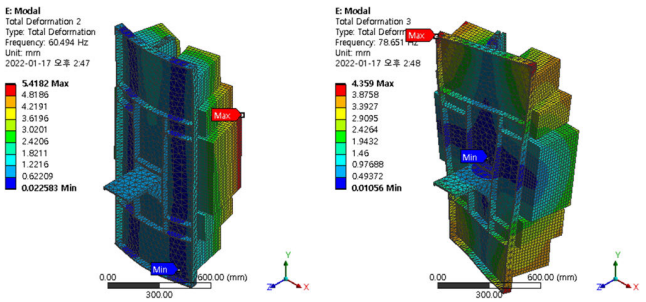

FIGURE 5. Vibration analysis of maglev ropeless elevator.

units at the backside corners of the elevator. Each maglev guiding unit is equipped with two X-axis electromagnets and one Y-axis electromagnet and gap sensors for acquiring the relative distance between the guide rail and electromagnet.

The four maglev guiding units generate 12 attractive forces, as shown in Fig. 2(Left). By superposing the attractive forces according to the action line, the individual forces can be simplified as 6 superposed forces, as shown in Fig. 2(Right). Because 6 superposed forces (f_1, f_2, f_3, f_4, f_5, and f_6) are used to control the 5 DOFs of the elevator (x, y, α, β, and γ), the control system can be said to be an overactuated system. Fig. 3 shows the arrangement of the electromagnets and gap sensors. The left and right guide rails are installed on the wall, and the maglev guiding units move along these guide rails. The gap sensor used was PU-05 with AEC-5505 converter from AEC Corp. This product features high resolution (0.3 μm) and excellent linearity ($\pm 0.5\%$/FS).

Based on the system model, including the effect of the eccentricity of the mass center from the lifting axis on the maglev guiding system, the required forces of the maglev guiding units can be calculated as shown in Table 1. Along the X- and Y-axes, the required forces are 335 N and 173 N,

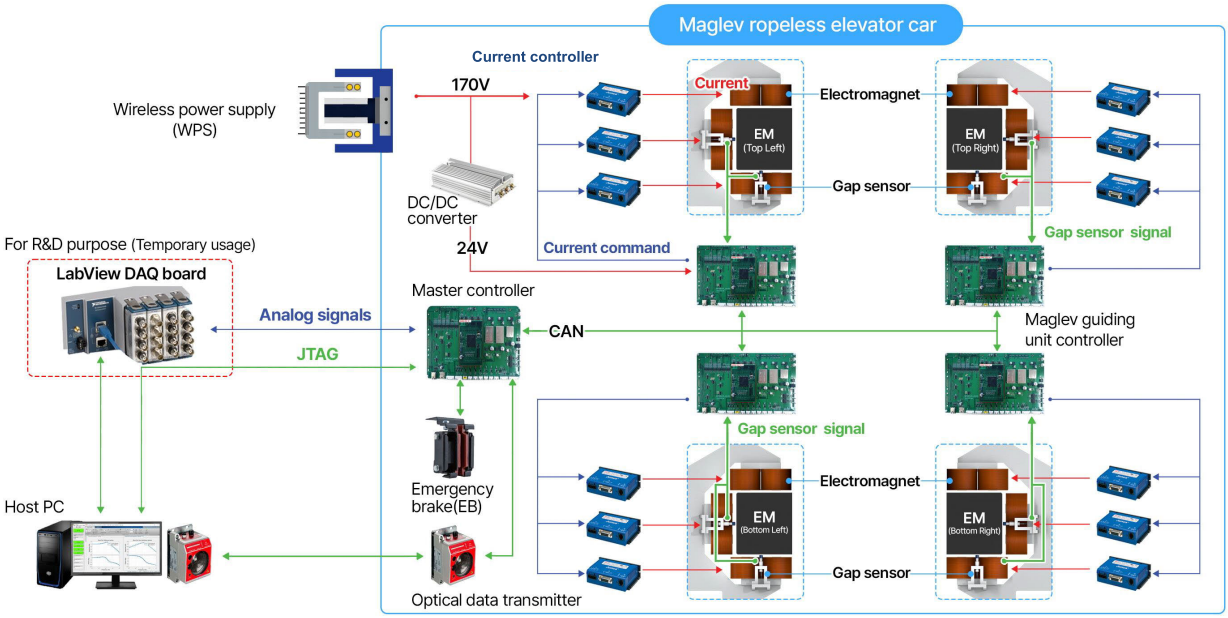

FIGURE 6. **Diagram of power and signal line connections.**

and the nominal values of the airgap are 0.9 mm and 0.7 mm, respectively. The maglev guiding units are designed with consideration of the available space, heat dissipation, and the inductances of the electromagnets which are closely related to the control bandwidth of the current control loop. The electromagnetic field distribution for the proposed maglev guiding units is shown in Fig. 4. The commercial inverter used was Junus JSP-180-20 from Copley Controls Corp. This allows precise current control up to a maximum of 20 A. In the experiment, the control bandwidth of the current control was set to be above 200 Hz. This is to satisfy the rule of thumb for cascade controller design that the inner loop control bandwidth should be sufficiently faster than the outer loop control bandwidth [15].

The lifting system consists of the armature of the LSM and the permanent magnet mover. To reduce the weight and power capacity of the elevator cabin, the armature coils and controller are placed on the ground, and the permanent magnets are placed on the elevator, as shown in Fig. 1. To control the lifting system, encoders, a linear scale, and limit sensors are used. A plurality of encoders are installed at evenly spaced intervals on the guide rail, and a linear scale is attached on the elevator. Based on the measured encoder signals, the Z-axis position of the elevator is calculated by the encoder synthesis algorithm. As a result of experimental evaluation, velocity control of the lifting system is performed with high control precision. Unfortunately, the LSM generates not only a lifting force in Z-direction but also a normal force in Y-direction acting as a disturbance on the maglev guiding control system as shown in Fig. 2(Left). According to experimental measurements, the magnitude of the normal force of the LSM is approximately 16% that of the lifting force and the normal force of the LSM increases proportionally with the lifting force. The normal force induces fluctuations in the Y and yaw directions of the elevator. Since the effect of the disturbance is expected to be critical in this system, the effect of the disturbance on airgap fluctuations should be considered when designing the maglev guiding system controller.

The maglev guiding units continuously adjust the attractive forces to maintain the airgaps at their nominal value. Therefore, maglev systems are inevitably vulnerable to resonance phenomena. When the force modulation frequency matches the natural frequency of the structure, the vibration of the structure significantly increases. To avoid resonance problems, the control bandwidth should be designed to be well below the natural frequency of the structure. In general, the higher the control bandwidth is, the better the control performance. To use a high control bandwidth without resonance problems, the rigidity of the structure must be increased. Increasing the structural rigidity increases the weight of the system and increases the size and capacity of the associated actuating parts, so the system engineer must make wise choices by considering a variety of trade-offs. Fig. 5 shows the structural analysis of the designed maglev guiding units and elevator frame. Efforts were made to ensure sufficient rigidity of the structure while minimizing the weight so that the lowest natural frequency is higher than 60 Hz. The dominant natural frequencies of the maglev ropeless elevator are 60.49 Hz (bending mode) and 78.65 Hz (twisting mode).

There are two types of controllers, called master and slave controllers, to control the maglev guiding units. The master controller monitors the control status of the slave controller and interfaces with external devices. The slave controller performs airgap control by adjusting the current

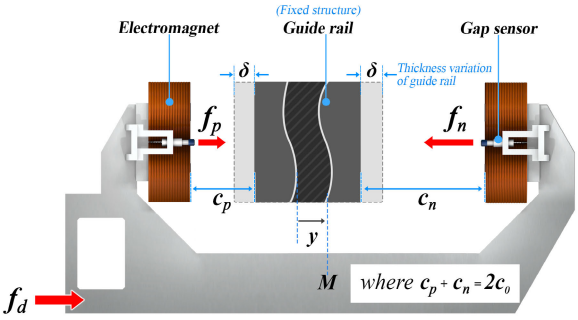

FIGURE 7. Simplified system model of the maglev guiding units (in the Y-direction).

applied to the electromagnets according to the gap sensor measurements. Fig. 6 shows the controller configuration and signal wiring. The red wiring is the power line. The high DC 170 V voltage from the WPS is supplied to each commercial inverter (JUNUS). The control board is supplied a DC 24 V voltage through a DC-DC converter. The blue wiring is the analog or pulse-width modulation (PWM) signal line. The purple wiring is the communication line such as CAN/JTAG. The master controller communicates with an external host PC using an optical communication device, and in an emergency situation, the emergency brake is used to keep the elevator safe. To collect experimental data, a data acquisition (DAQ) board is used only temporally for the test operation to monitor and save the internal variables of the master and slave controllers.

III. MAGLEV GUIDING SYSTEM

A. SYSTEM MODELING

As described in the previous section, the vertical movement of the elevator is controlled by the LSM, and the horizontal movement is controlled by the maglev guiding units. The maglev controllers adjust the current applied to the electromagnets based on the airgap measurements so that the maglev ropeless elevator maintains a constant airgap in the X/Y-direction. Strictly speaking, there is a mechanical coupling effect between the individual maglev guiding units, but when the system is simplified, the interaction between the maglev guiding units and the guide rail can be represented as shown in Fig. 7, and its equation of motion can be written as

$$m\ddot{y} = f_p - f_n + f_d, \tag{1}$$

where m is the effective mass of the maglev ropeless elevator and y is the movement of the maglev ropeless elevator in the Y-direction. For the movement of the maglev ropeless elevator in the X-direction, y is replaced by x. f_p and f_n are the positive and negative attractive forces generated by the electromagnets installed at opposite corners, as shown in Fig. 2, and f_d is the disturbance force. The effective mass (m) depends on the X/Y-axis. In the case of the X-axis, since 4 sets of electromagnets are involved in X-axis movement, the effective mass (m) is 1/4 of the total mass ($M = 298.9$ kg) of the maglev ropeless elevator. In contrast, in the case of the Y-axis, the effective mass (m) is 1/2 of the total mass.

As mentioned in [16], the magnitude of the attractive force generated by an electromagnet can be written as

$$f(i, c) = \frac{\mu_0 {N_e}^2 A}{4}\left[\frac{i}{c}\right]^2. \tag{2}$$

The attractive force is determined by the vacuum permeability ($\mu_0 = 4\pi \times 10^{-7}$H/m), number of windings (N_e), pole area of the electromagnet (A), applied current (i), and airgap (c). For linear controller design, (1) is linearized at the operation point (i_0, c_0) as

$$m\ddot{y} = k_i\left(\Delta i_p - \Delta i_n\right) + 2\,k_c y + f_d, \tag{3}$$

where $\Delta i_p = i_p - i_0$ and $\Delta i_n = i_n - i_0$. Assuming that there is no thickness variation of the guide rail ($\delta = 0$), $y = c_0 - c_p = c_n - c_0$. $k_i = \frac{\mu_0 {N_e}^2 A i_0}{2{c_0}^2}$, and $k_c = \frac{\mu_0 {N_e}^2 A {i_0}^2}{2{c_0}^3}$. k_i and k_c are obtained from $\frac{\partial f}{\partial i}$ and $\frac{\partial f}{\partial c}$ at the operation point [17]. Therefore, k_i and k_c are greatly affected by the operation point. In motor control, k_i and k_c play the same role as the torque constant and back electromotive force (EMF) constant.

B. CONTROL DESIGN

The controller is designed so that the maglev ropeless elevator can maintain a constant airgap from the guide rail in the X/Y-direction. Based on (3), Fig. 8 shows a block diagram of transforming the maglev guiding control system using the Laplace transform. In this study, a controller is designed using the PID structure.

$$\mathbf{I_{ref}} = \underbrace{\left(K_P + K_I\frac{1}{s} + K_D\frac{K_N s}{s + K_N}\right)}_{\mathbf{C}}\mathbf{E} = \mathbf{C}\left(\mathbf{Y_d} - \mathbf{Y} - \mathbf{N}\right). \tag{4}$$

For the integral controller, the clamping method with the integral limit suggested in [18] is used to prevent the anti-windup problem. The control performance of the designed feedback system is determined as follows:

$$\mathbf{Y} = \frac{\mathbf{L}}{1 + \mathbf{L}}\left(\mathbf{Y_d} - \mathbf{N}\right) + \frac{\mathbf{G}}{1 + \mathbf{L}}\mathbf{F_d}, \tag{5}$$

where $\mathbf{K} = 2k_i$, $\mathbf{G} = \frac{1}{ms^2 - 2k_c}$, and loop gain $\mathbf{L} = \mathbf{GCK}$.

The tracking error defined as the difference between the output and reference can be written as

$$\begin{aligned}\mathbf{E}_t &= \mathbf{Y_d} - \mathbf{Y} \\ &= \mathbf{S}\left(\mathbf{R} - \mathbf{GF_d}\right) + \mathbf{TN},\end{aligned} \tag{6}$$

where $\mathbf{S} = \frac{1}{1+\mathbf{L}}$ and $\mathbf{T} = \frac{\mathbf{L}}{1+\mathbf{L}}$ are the sensitivity and complementary sensitivity functions, respectively. In addition, there is a constraint of $\mathbf{S} + \mathbf{T} = 1$. For the tracking error $\mathbf{E}_t = 0$ with arbitrary input, $\mathbf{S} = \mathbf{T} = 0$ should hold, but such a solution does not exist. Alternatively, the feedback controller is designed using the loop shaping technique [15]. In the low-frequency range, the magnitude of the loop gain

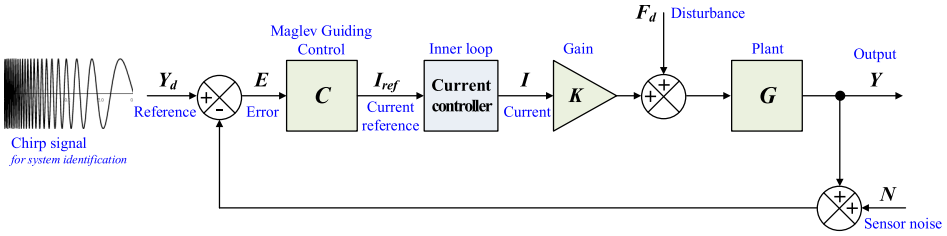

FIGURE 8. Block diagram of the maglev guiding control system.

is designed to be higher than a certain level in consideration of disturbance attenuation and tracking performance, whereas in the high-frequency range, the magnitude of the loop gain is designed to be lower than a certain level in consideration of minimizing the unmodeled dynamic effect and the noise attenuation performance.

To prevent resonance problems caused by the interaction between the control bandwidth of the feedback system and vibration mode of the elevator, as mentioned in [19], the control bandwidth of the maglev guiding units should be designed to be smaller than the dominant natural frequencies of the system. In this study, the control bandwidth is designed to be less than 30 Hz, taking into account the dominant natural frequencies of 60.49 Hz (bending mode) and 78.65 Hz (twisting mode) as described in the previous section.

In this system, most of the external disturbance is caused by the normal force of the LSM. This force is generated in the Y-direction, and its magnitude increases with the lifting acceleration. Under a given operating condition (refer to Table 2), the disturbance caused by the normal force of the LSM remains below 280 N. At this time, for control stability, the tracking error should not exceed the nominal airgap. The disturbance frequency is determined by the pole pitch of the permanent magnet of the LSM and the lifting speed. A higher lifting speed results in a higher disturbance frequency. Therefore, to minimize the effect of external disturbance on airgap variation, the feedback controller should be designed with $|\mathbf{GS}| < -110$ dB over all frequency ranges.

In the controller design, considering not only the absolute stability of the feedback system but also a sufficient level of relative stability is very important to guarantee the control performance during long-term operation with changes in system characteristics. Moreover, the phase margin is one of the key factors determining the transient response characteristics. Therefore, in this study, the phase margin was designed to be at least 45 degrees.

The current controller exists in the form of an inner loop in the maglev guiding control, and to minimize its impact on maglev guiding control, the bandwidth of the current controller has been set to 200 Hz.

IV. EXPERIMENTAL EVALUATION

A. SYSTEM IDENTIFICATION: SINE SWEEP TEST

To verify the control performance after designing the maglev guiding control, a sine sweep vibration experiment was performed to analyze the frequency response characteristics. The amplitude of the chirp signal added to the reference input was set to ±0.05 mm, and the frequency of the chirp signal was changed from 100 Hz to 0.1 Hz over 60 seconds. Fig. 9(a) shows the reference input with the chirp signal, airgap measurement, and reference of the current while performing a sine sweep vibration test in the X-direction. Similarly, Fig. 9(b) shows the data obtained while performing the sine sweep vibration test in the Y-direction.

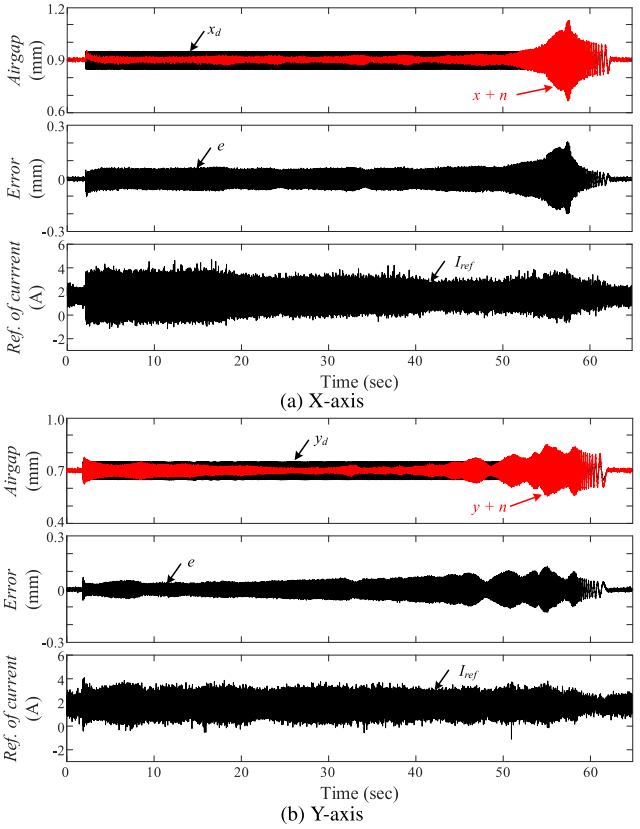

FIGURE 9. Sine sweep vibration tests in the X/Y-direction.

Fig. 10(a,b) shows estimated Bode plots of reference vs. output measurement and error vs. output measurement based on the measurement data from the sine sweep vibration experiment. As shown in (5), theoretically, the transfer function of the reference and output measurement (error and output measurement) has a 4^{th}-order form in

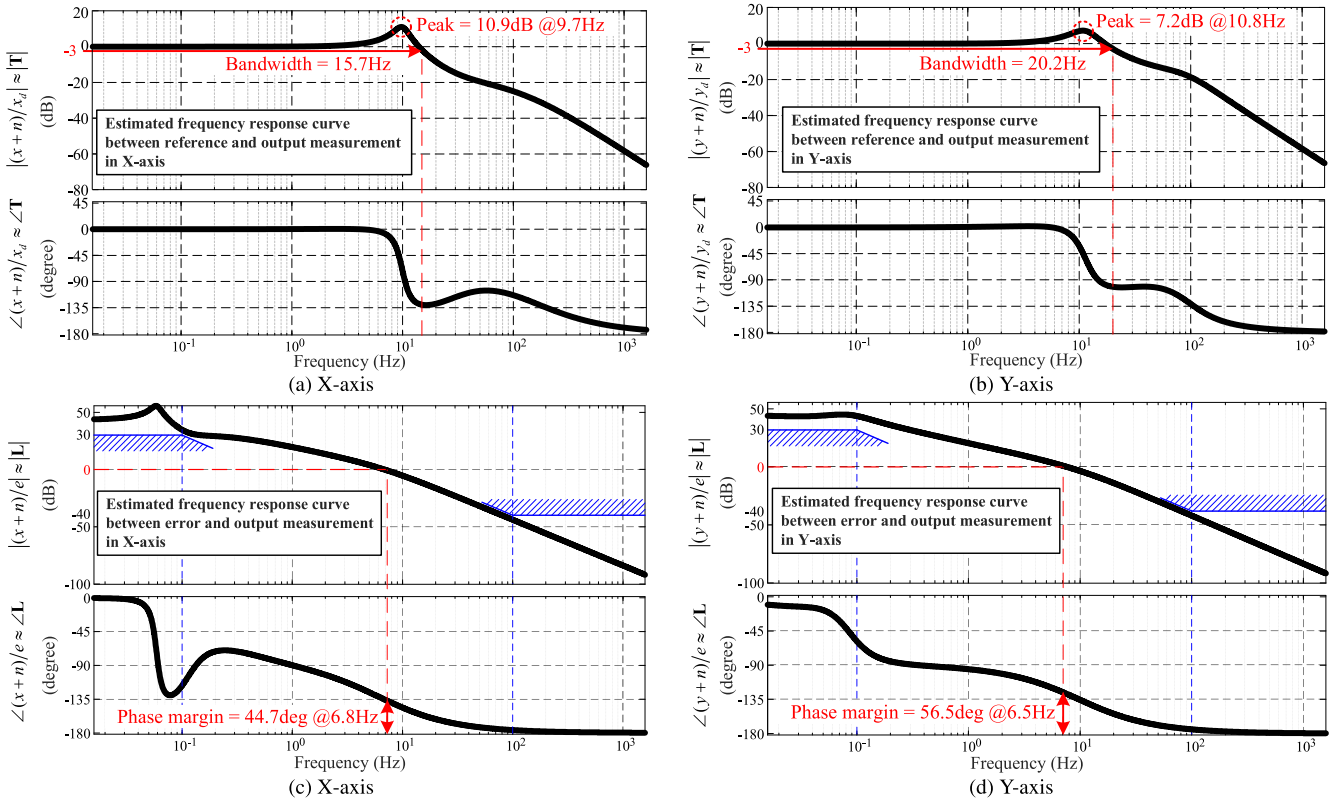

FIGURE 10. (a,b) Estimated frequency response curves between reference and output and (c,d) error and output in the X/Y-axis based on measurement data from sine sweep vibration tests.

the denominator and a 2^{nd}-order form in the numerator. Therefore, when estimating a transfer function using the MATLAB System Identification Toolbox, information about the order of the transfer function and the frequency bandwidth of interest was taken into account to minimize experimental error.

As shown in Fig. 10(a,b), the control bandwidth of the developed feedback system is 15.7 Hz on the X-axis and 20.2 Hz on the Y-axis. As shown in Fig. 10(c,d), the phase margins of the developed feedback system are 44.7 degrees on the X-axis and 56.5 degrees on the Y-axis. The phase margin was confirmed to be actually implemented similar to or larger than our designed value (45 degrees). Based on linear feedback control theory [15], the developed maglev control system is stable, as evidenced by the positive gain and phase margins.

In the high-frequency range (>100 Hz), a smaller $|\mathbf{L}|$ means better sensor noise attenuation performance. In the case of the developed feedback system, as shown in Fig. 10(c,d), $|\mathbf{L}|$ is confirmed to be less than -40 dB in the high-frequency range on the X/Y-axis.

In the low-frequency range (<0.1 Hz), a higher $|\mathbf{L}|$ means better tracking performance and disturbance rejection performance. In the case of the developed feedback system, as shown in Fig. 10(c,d), $|\mathbf{L}|$ is confirmed to be larger than 30 dB in the low-frequency range on the X/Y-axis.

TABLE 2. Lifting conditions of the maglev ropeless elevator.

Parameter	Description	Lifting condition I	Lifting condition II
D	Lifting distance	3000 mm	
$V_{\max}$	Max. velocity	1600 mm/s	2600 mm/s
$A_{\max}$	Max. acceleration	2000 mm/s^2	

The transient response characteristics of the developed feedback system are determined by the phase margin and peak value of $|\mathbf{T}|$. In general, the transient response characteristics improve as the phase margin increases and the peak value decreases, but there is a trade-off between the transient response characteristics and other control performance parameters unless the structure of the controller is changed. Therefore, control engineers must optimize the loop shape by adjusting the control gains in a constrained environment.

B. DRIVING TEST: TWO DIFFERENT LIFTING CONDITIONS

To experimentally verify the control performance of the developed maglev guiding units when the maglev ropeless elevator is driven in the Z direction, we analyzed the behavior of the maglev guiding units under two different lifting conditions, as shown in Table 2. The maglev ropeless elevator repeatedly travels up and down from 900 mm to 3900 mm in the Z direction. The lifting distance (D) is 3000 mm.

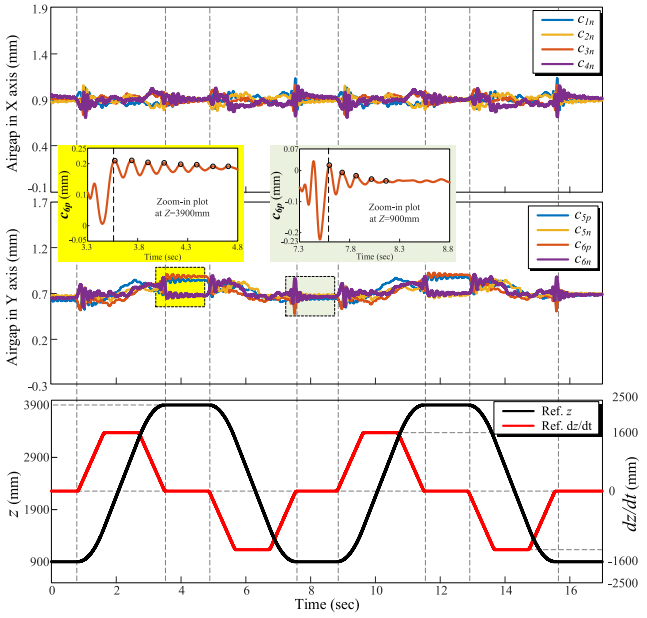

FIGURE 11. Airgap measurement and Z-axis movement of the maglev ropeless elevator under lifting condition I.

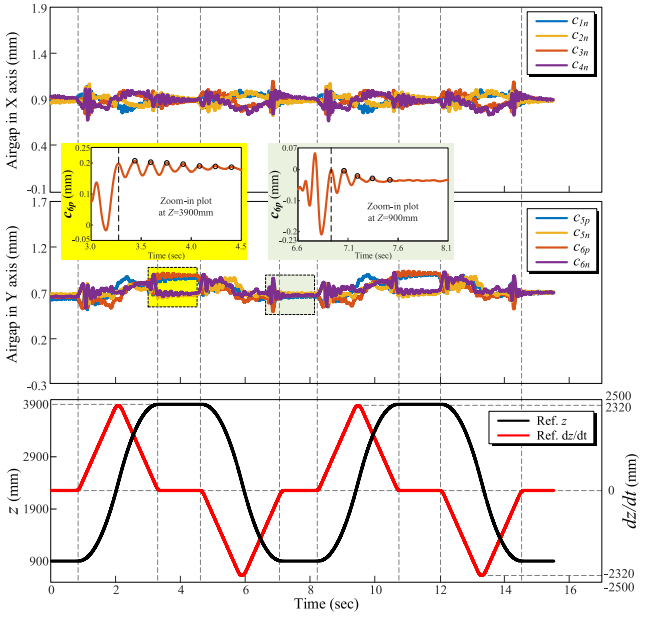

FIGURE 12. Airgap measurement and Z-axis movement of the maglev ropeless elevator under lifting condition II.

The maximum lifting velocity ($V_{\max}$) is 1600 mm/s in lifting condition I, and the elevator travels faster in lifting condition II, with $V_{\max} = 2600$ mm/s. The acceleration and deceleration periods are symmetric, and the maximum acceleration ($A_{\max}$) is 2000 mm/s^2 under both lifting conditions. Figs. 11-12 (bottom) show the Z-axis position and velocity commands based on the S-curve motion profile generation described in [20]. The ratio of the constant jerk and acceleration periods is 2:8.

Figs. 11-12 (top, bottom) show the behavior in the X/Y direction of the maglev ropeless elevator under the

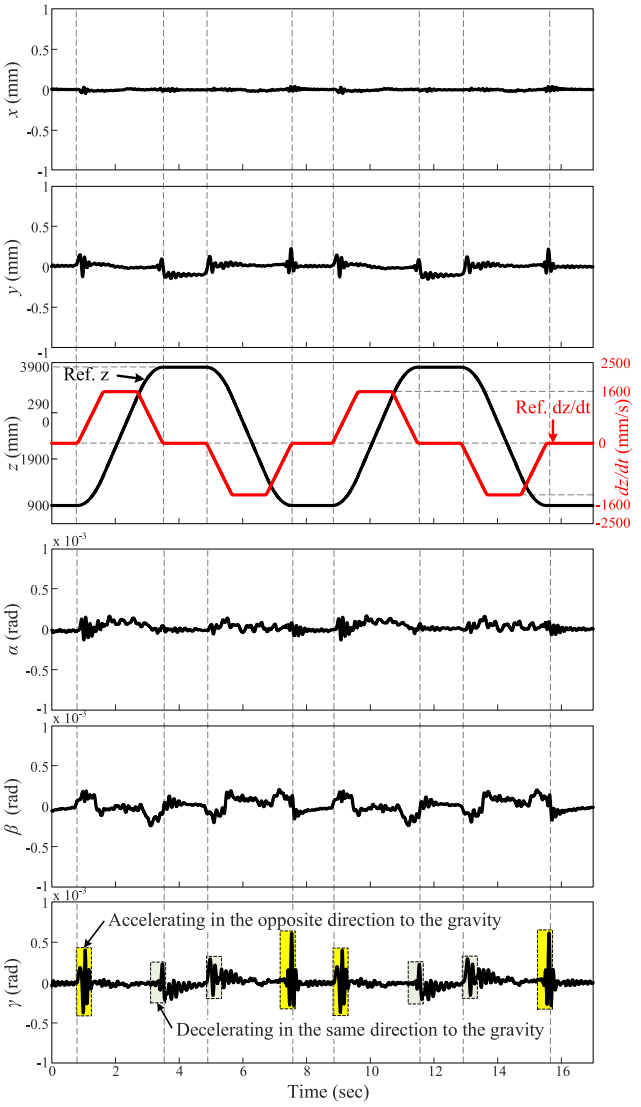

FIGURE 13. 5 DOFs of the maglev ropeless elevator transformed from airgap measurements under lifting condition I.

two different lifting conditions. Under both conditions, the maximum airgap variation is less than ±0.2 mm, which is satisfactory and is very small compared to the gap between the electromagnets and the guide rail. That is, the maglev guiding units are well controlled without any physical contact when the elevator moves in the Z direction.

As shown in Fig. 3, in the case of the Y-axis, the electromagnets are far apart from each other, unlike in the X-axis case. This means that constantly managing the guide rail thickness is not easy. In fact, as shown in Figs. 11-12 (middle), all airgaps are the nominal value ($c_0 = 0.7$ mm) at $z = 900$ mm, whereas c_{5p} (c_{6p}) is larger than the nominal value at $z = 3900$ mm. This means that the thickness of the guide rail decreases as the elevator goes up along the Z-axis. The thickness variation of the guide rail means that the operation point of the airgap in the Y-direction changes from c_0 to $c_0 + \delta$ while keeping the airgap reference. In (3),

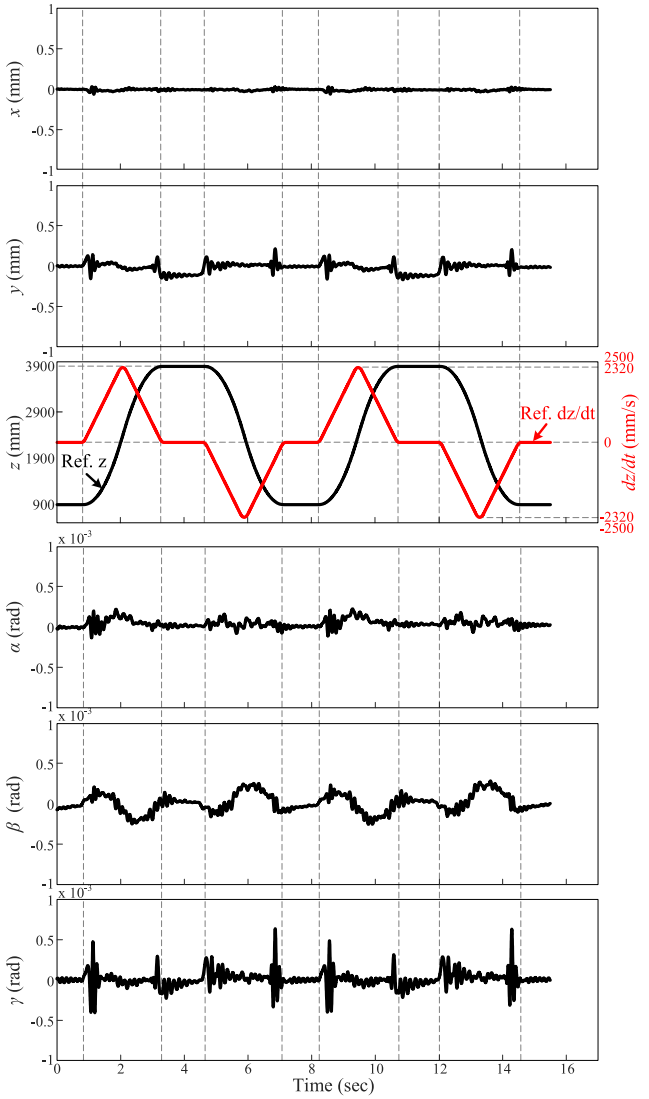

FIGURE 14. 5 DOFs of the maglev ropeless elevator transformed from airgap measurements under lifting condition II.

k_i and k_c become small due to the change in the operation point. In terms of the control performance, the phase margin decreases, and the transient response characteristics are degraded. For example, as shown in Figs. 11-12 (middle), the time required for natural attenuation of vibration after arrival at $z = 3900$ mm is longer than that after arrival at $z = 900$ mm. In this simulation, the phase margin was confirmed to be decreased by approximately 7 degrees when the operation point changed by 15% due to the change in rail thickness. Therefore, implementing sufficient relative stability is very important to guarantee the control performance even when the system characteristics change under harsh operation conditions.

The experimental data in Figs. 11-12 are the local movement of four corner of the maglev ropeless elevator measured by the gap sensors. The 5 DOFs of the maglev ropeless elevator at the mass center can be calculated from airgap measurements. For example, assuming that the

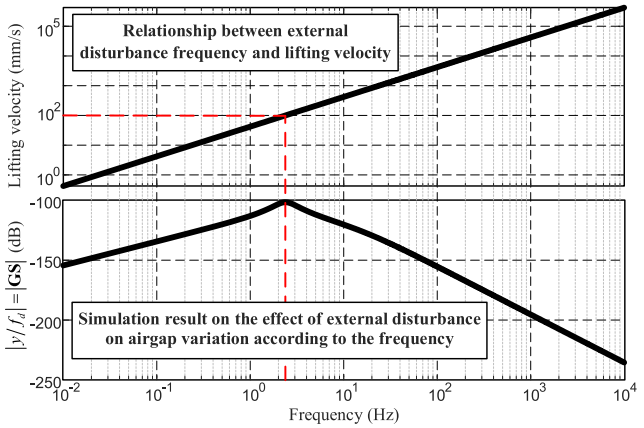

FIGURE 15. (Top) Relationship between the external disturbance frequency and lifting velocity, and (bottom) simulation result of the effect of the external disturbance on airgap variation according to the frequency.

rotation movement is small, Roll (α), Pitch (β), and Yaw (γ) can be obtained as

$$\alpha = \frac{c_{5p} - c_{5n} - c_{6p} + c_{6n}}{4h}$$
$$\beta = \frac{c_{1n} + c_{2n} - c_{3n} - c_{4n}}{4h}$$
$$\gamma = \frac{c_{1n} - c_{2n} + c_{3n} - c_{4n}}{4w}. \quad (7)$$

The translation movements in the X- and Y-directions are as

$$x = \frac{c_{1n} + c_{2n} + c_{3n} + c_{4n}}{4} - c_0$$
$$y = \frac{-c_{5p} + c_{5n} - c_{6p} + c_{6n}}{4} + d\gamma \quad (8)$$

where h, w, and d are the vertical distance in the Z-direction, horizontal distance in the Y-direction horizontal distance in the X-direction between the mass center and electromagnet as shown in Fig. 2 (Left).

Figs. 13-14 show the 5 DOFs of the maglev ropeless elevator. In translation movement, the fluctuation in the Y-direction is greater than that in the X-direction, and in rotational movement, the fluctuation in yaw is greater than that in roll and pitch. This is because the main factor in the airgap fluctuation is the normal force of the LSM acting along the Y-axis at the position d away from the mass center in the X-direction. As explained in the previous section, the normal force of the LSM increases as the lifting force increases. As seen from the yaw movement in Fig. 13, accelerating (or decelerating) in the opposite direction to gravity requires more lifting force, resulting in greater fluctuations than when accelerating (or decelerating) in the same direction as gravity.

Fig. 15 shows the relationship between the external disturbance frequency and lifting velocity and the simulation result of the effect of the external disturbance on the airgap variation $|\mathbf{GS}|$ according to the frequency. The external disturbance has the greatest effect on the airgap variation around a lifting velocity of 100 mm/s, and the effect on the

TABLE 3. Riding performance of the maglev ropeless elevator.

Parameters	Description	Lifting Condition I	Lifting Condition II
x_p	Max. translation in X	0.044 mm	0.057 mm
y_p	Max. translation in Y	0.224 mm	0.227 mm
α_p	Max. rotation in roll	1.51e-04 rad	1.99e-04 rad
β_p	Max. rotation in pitch	2.47e-04 rad	2.80e-04 rad
γ_p	Max. rotation in yaw	6.16e-04 rad	6.28e-04 rad

airgap variation significantly decreases as the lifting velocity increases. Similar to the simulation results, as shown in Figs. 13-14, there is a slight airgap fluctuation during low-speed operation, and the airgap is stabilized when the lifting velocity is increased. For this reason, maglev guiding system is effective at high speed operation.

As shown in Figs. 13-14, the pitch motion is the effect of moment caused by the offset d between the mass center and the lifting force. Such pitch fluctuation can be reduced if the lifting force can be designed to be closer to the mass center.

Table 3 summarizes the maximum fluctuations in 5 DOFs (riding performance) of the maglev ropeless elevator in each lifting condition. The maximum translation fluctuation for X/Y-axis is less than 0.23 mm, and the maximum rotation fluctuation in roll, pitch, and yaw is less than 6.3e-04 rad (0.036 degrees), which is very small compared to the nominal airgap. This shows how the maglev guiding system can achieve a high level of riding quality in harsh environments, such as under misalignment and disconnection of the guide rail segments and high-speed operation, thanks to the contactless driving.

V. CONCLUSION

A ropeless elevator with a maglev guiding system and an LSM for semiconductor wafer vertical transport was designed based on a robust feedback control. The main consideration for the elevator is the eccentricity of the mass center from the lifting axis due to space limitations. High acceleration/deceleration operation generates a large amount of pitch motion of the elevator car. Furthermore, periodic large disturbances from the normal force of the linear synchronous motor, resonance of the elevator car, and manufacturing tolerance of the guide rail exist in the prototype of the maglev ropeless elevator. To satisfy the ride performance for various driving conditions, the loop shape of the designed maglev guiding control is adjusted in consideration of vibration analysis of the system, sensor noise and disturbance characteristics, and transient responses. In particular, to guarantee the control performance even when the thickness of the guide rail changes, the phase margin is designed to be higher than 45 degrees. According to experimental evaluations with full-scale maglev ropeless elevator prototype under harsh operation conditions ($V_{max} = 2600$ mm/s), the maximum translation fluctuation in horizontal movement is less than 227 μm, and the maximum rotation fluctuation in roll, pitch, and yaw is less than 0.036 degrees, which are very small compared to the nominal airgap. In future work, better control performance is expected to be achieved if a controller based on a detailed dynamic model is developed and a disturbance observer is applied to minimize the effect of external disturbances in the low-frequency range.

REFERENCES

[1] B. Zhao, Z. Quan, Y. W. Li, L. Quan, Y. Hao, and L. Ding, "A hybrid-driven elevator system with energy regeneration and safety enhancement," *IEEE Trans. Ind. Electron.*, vol. 67, no. 9, pp. 7715–7726, Sep. 2020.

[2] L. Guo, Q. Zhou, M. Galea, and W. Lu, "Cogging force optimization of double-sided tubular linear machine with tooth-cutting," *IEEE Trans. Ind. Electron.*, vol. 69, no. 7, pp. 7161–7169, Jul. 2022.

[3] R. Appunn, J. Frantzheld, M. Jetter, and F. Löser, "MULTI®–rope-less elevator demonstrator at test tower rottweil," *Transp. Syst. Technol.*, vol. 4, no. 3, pp. 80–89, Nov. 2018.

[4] A. Onat, E. Kazan, N. Takahashi, D. Miyagi, Y. Komatsu, and S. Markon, "Design and implementation of a linear motor for multicar elevators," *IEEE/ASME Trans. Mechatronics*, vol. 15, no. 5, pp. 685–693, Oct. 2010.

[5] Y. Okamoto and N. Takahashi, "Minimization of driving force ripple of linear motor for rope-less elevator using topology optimization technique," *J. Mater. Process. Technol.*, vol. 181, nos. 1–3, pp. 131–135, Jan. 2007.

[6] A. Zahid, F. Khan, N. Ahmad, I. Sami, W. Ullah, N. Ullah, N. Ullah, and H. I. Alkhammash, "Design and analysis of dual mover multi-tooth permanent magnet flux switching machine for ropeless elevator applications," *Actuators*, vol. 10, no. 4, p. 81, Apr. 2021.

[7] H. S. Lim and R. Krishnan, "Ropeless elevator with linear switched reluctance motor drive actuation systems," *IEEE Trans. Ind. Electron.*, vol. 54, no. 4, pp. 2209–2218, Aug. 2007.

[8] D. Wang, X. Du, D. Zhang, and X. Wang, "Design, optimization, and prototyping of segmental-type linear switched-reluctance motor with a toroidally wound mover for vertical propulsion application," *IEEE Trans. Ind. Electron.*, vol. 65, no. 2, pp. 1865–1874, Feb. 2018.

[9] I. Hiroaki, M. Mimpei, and Y. Akira, "Magnetic suspension system for elevators," *Toshiba Rev.*, vol. 62, no. 5, pp. 10–13, 2007.

[10] H. Alipour, M. B. B. Sharifian, and H. Afsharirad, "A PID sliding mode control for ropeless elevator Maglev guiding system," *Energy Power Eng.*, vol. 4, no. 3, pp. 158–164, 2012.

[11] B. Schmulling, R. Appunn, and K. Hameyer, "Electromagnetic guiding of vertical transportation vehicles: State control of an over-determined system," in *Proc. 18th Int. Conf. Electr. Mach.*, Sep. 2008, pp. 1–6.

[12] R. Appunn, B. Schmulling, and K. Hameyer, "Electromagnetic guiding of vertical transportation vehicles: Experimental evaluation," *IEEE Trans. Ind. Electron.*, vol. 57, no. 1, pp. 335–343, Jan. 2010.

[13] R. Appunn and K. Hameyer, "Modern high speed elevator systems for skyscrapers," in *Proc. Maglev*, Sep. 2014, p. 24.

[14] R. Appunn and K. Hameyer, "Contactless power supply for magnetically levitated elevator systems using a SMC hybrid actuator," in *Proc. Int. Conf. Electr. Mach. (ICEM)*, Sep. 2014, pp. 436–442.

[15] K. A. Morris, *Introduction to FeedBack Control*. New York, NY, USA: Academic Press, 2000.

[16] J. Kim, G. B. King, C.-H. Kim, and C.-W. Ha, "Modeling and designing levitation, roll and pitch controller for high accuracy Maglev tray system," *Mechatronics*, vol. 53, pp. 181–191, Aug. 2018.

[17] J. Kim, G. B. King, C.-H. Kim, and C.-W. Ha, "Experimental validation of deadzone compensation for a magnetic levitation transporting OLED displays system," *Int. J. Control, Autom. Syst.*, vol. 20, no. 9, pp. 2937–2947, Sep. 2022.

[18] A. Visioli, "Modified anti-windup scheme for PID controllers," *IEE Proc. Control Theory Appl.*, vol. 150, no. 1, pp. 49–54, Jan. 2003.

[19] J. Kim, C.-W. Ha, G. B. King, and C.-H. Kim, "Experimental development of levitation control for a high-accuracy magnetic levitation transport system," *ISA Trans.*, vol. 101, pp. 358–365, Jun. 2020.

[20] C.-W. Ha and D. Lee, "Analysis of embedded prefilters in motion profiles," *IEEE Trans. Ind. Electron.*, vol. 65, no. 2, pp. 1481–1489, Feb. 2018.

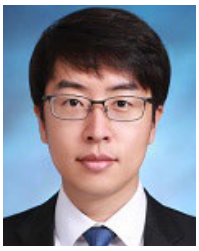

CHANG-WAN HA (Member, IEEE) received the B.S. degree in mechanical engineering from Handong Global University, Pohang, Republic of Korea, in 2008, and the M.S. and Ph.D. degrees in mechanical engineering from the Korea Advanced Institute of Science and Technology (KAIST), Daejeon, Republic of Korea, in 2010 and 2014, respectively.

Since 2014, he has been a Senior Researcher with the Korea Institute of Machinery and Materials (KIMM). Since 2023, he has been an Associate Professor with KIMM, University of Science and Technology (UST). His research interests include magnetic levitation and linear propulsion systems and motion control including the input-shaping technique.

SUNGHO JUNG (Member, IEEE) received the B.S. degree in electronic and electrical engineering from Pusan National University, in 2010, and the M.S. and Ph.D. degrees in electrical and computer engineering from Seoul National University (SNU), Seoul, Republic of Korea, in 2012 and 2016, respectively.

He was a Senior Researcher with Hyundai Mobis Company Ltd., Seoul, from 2016 to 2019. Since 2019, he has been a Senior Researcher with the Korea Institute of Machinery and Materials (KIMM). His research interests include electric machine drives and magnetic levitation systems.

JINSEONG PARK (Member, IEEE) received the B.S., M.S., and Ph.D. degrees in mechanical engineering from the Korea Advanced Institute of Science and Technology (KAIST), Daejeon, Republic of Korea, in 2008, 2010, and 2016, respectively.

He was a Senior Researcher with Hyundai Robotics Company Ltd., Ulsan, Republic of Korea, from 2016 to 2017. Since 2017, he has been a Senior Researcher with the Korea Institute of Machinery and Materials (KIMM). His research interests include optimal control, active vibration control, and fault diagnosis, with an emphasis on mobile manipulators, vehicles, and magnetic levitation systems.

JAEWON LIM (Member, IEEE) received the B.S., M.S., and Ph.D. degrees in electrical and computer engineering from Seoul National University (SNU), Seoul, Republic of Korea, in 2004, 2006, and 2011, respectively.

Since 2011, he has been a Principal Researcher with the Korea Institute of Machinery and Materials (KIMM). His research interests include design of magnetic levitation and linear propulsion systems.